INTERNATIONAL JOURNAL FOR NUMERICAL METHODS IN FLUIDS
Int. J. Numer. Meth. Fluids 2004; **45**:1269–1289 (DOI: 10.1002/fld.596)

A numerical-variational procedure for laminar flow in curved square ducts

P. M. Hatzikonstantinou*,† and V. D. Sakalis

Department of Engineering Science, University of Patras, GR 26500 Patras, Greece

SUMMARY

A new numerical method is presented for the solution of the Navier–Stokes and continuity equations governing the internal incompressible flows. The method denoted as the CVP method consists in the numerical solution of these equations in conjunction with three additional variational equations for the continuity, the vorticity and the pressure field, using a non-staggered grid. The method is used for the study of the characteristics of the laminar fully developed flows in curved square ducts. Numerical results are presented for the effects of the flow parameters like the curvature, the Dean number and the stream pressure gradient on the velocity distributions, the friction factor and the appearance of a pair of vortices in addition to those of the familiar secondary flow. The accuracy of the method is discussed and the results are compared with those obtained by us, using a variation of the velocity–pressure linked equation methods denoted as the PLEM method and the results obtained by other methods. Copyright © 2004 John Wiley & Sons, Ltd.

KEY WORDS: internal flow; numerical CVP method; incompressible flow

1. INTRODUCTION

The flow through curved ducts is extensively used in industrial applications and particularly in various heat and mass transfer apparatuses, heat apparatus, aircraft intakes and in blood flow through the arteries. The flow in curved ducts is characterized by the secondary flow which is developed in the cross-sectional plane normal to the axial direction, from the action of the centrifugal force. Analytical efforts for the solution of the problem have been carried out by Dean [1], Mc Conaloque *et al.* [2], Greenspan [3], Srivastava [4], Topakoglou *et al.* [5], using perturbative techniques and by Mori *et al.* [6, 7] using integral methods for small and large Dean numbers. The extension of these approximated dynamical results to the study of heat transfer yielded equally approximated results. Experimental results have been obtained by Ito [8] and Balejova *et al.* [9].

*Correspondence to: P. M. Hatzikonstantinou, Department of Engineering Science, University of Patras, GR 26500 Patras, Greece.
†E-mail: hatzikon@upatras.gr

Published online 25 May 2004

Received 7 September 2002
Revised 14 April 2003

However, detailed studies for the effects of the main parameters like the curvature κ, the Dean number, the Reynolds number and the axial pressure gradient on the curved flow, have been carried out computationally applying various numerical methods. The fully developed incompressible laminar flow in curved rectangular ducts has been studied numerically by Cheng *et al.* [10], Hwang *et al.* [11], Ghia *et al.* [12] and Kamiyama [13] within the stream function-vorticity formalism by Dong and Ebadian [14] and Thangam and Hur [15] applying the SIMPLE method and by Duh *et al.* [16] studying the fully developed flow in curved channels of inclined cross-sections using primitive variables. More information about the internal flow in curved ducts with circular, and rectangular cross-sections are found in the review article published by Berger *et al.* [17].

Various numerical methods have been implemented for the study of internal flows. Numerical methods based on the vorticity-stream function formalism are appropriate for two-dimensional flow problems but they cannot easily be generalized to three-dimensional problems or to problems with curvilinear co-ordinate systems. On the other hand numerical procedures based on the pressure linked equations of the velocity primitive variables, like the MAC or SIMPLE methods, are based on the adoption of staggered grids for the avoidance of spurious oscillations from the solutions, increasing substantially the mathematical difficulties and particularly in problems of complex geometries.

The objective of this work is the application of a new numerical method developed by us [18, 19] which in addition to the continuity and momentum equations, involves an additional set of variational representations of the continuity, vorticity and pressure equations and is denoted, by their acronym, as the CVP variational method. The predictions and accuracy of the method, are examined studying the incompressible fully developed laminar flow in curved ducts. The advantages of the method are the use of a non-staggered grid for primitive variables without the introduction of spurious oscillation in the solutions and its easy application to problems of complex geometries. For a better understanding of the proposed method, our CVP results are compared with the results obtained also by us, applying a variation of the pressure linked equation methods, denoted as the PLEM method, incorporating also a non-staggered grid. Our results are also compared with those obtained by other methods.

2. PROBLEM FORMULATION

We consider a curved square duct of width a and radius of curvature R_c with respect to a Cartesian reference system (X, Y, Z), the co-ordinates of which are transformed to the toroidal co-ordinate system (s', x', y') as shown in Figure 1 via the relations

$$X = (R_c - x')\cos(s'/R_c), \quad Z = (R_c - x')\sin(s'/R_c), \quad Y = y' \tag{1}$$

The velocity $\mathbf{V}' = (u_1', u_2', u_3')$ where u_1' and u_2', u_3' are the axial and transverse components along the directions s' and x', y', respectively, and the pressure p' satisfies the momentum Navier–Stokes and the continuity equations. In the fully developed laminar incompressible flow the pressure gradient varies only along the cross-section of the duct, while it is constant along the axial direction. Thus, the pressure splits into two terms $p' = p^{a'}(s') + p'(x', y')$ where the pressure gradient $p^a_{s'} = \partial p^a / \partial s'$ in the axial direction, is considered as constant. Besides, the axial derivatives of the velocity components are considered negligible.

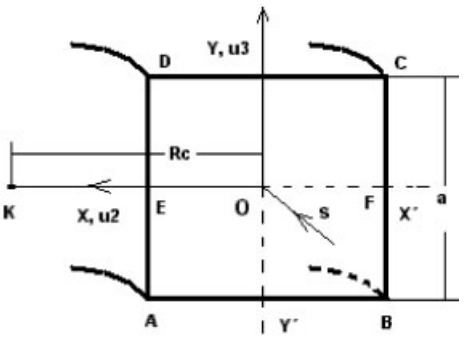

Figure 1. Co-ordinates and physical configuration.

In terms of the non-dimensional variables and parameters

$$x=\frac{x'}{a},\ y=\frac{y'}{a},\ s=\frac{s'}{a},\ u_1=\frac{u_1'a}{v},\ u_2=\frac{u_2'a}{v},\ u_3=\frac{u_3'a}{v}$$
$$p=\frac{p'}{\rho v^2/a^2},\ t=\frac{t'\mu}{\rho a^2},\ \kappa=\kappa' a=\frac{a}{R_c},\ J=\frac{1}{1-\kappa x}=J'=\frac{1}{1-\kappa' x'} \tag{2}$$

where t' is the time, v is the kinematic viscosity, κ the curvature. Defining $\partial p/\partial x = p_x$ and $\partial p/\partial y = p_y$ the non-dimensional governing equations of the problem take the following form:

Continuity equation

$$\frac{\partial u_2}{\partial x}+\frac{\partial u_3}{\partial y}-\kappa J u_2=0 \tag{3}$$

The s-momentum equation

$$\frac{\partial u_1}{\partial t}+\frac{\partial (u_1u_2)}{\partial x}+\frac{\partial (u_3u_1)}{\partial y}-2\kappa J u_1u_3=-Jp_s^{\mathrm{a}}+\frac{\partial^2 u_1}{\partial x^2}+\frac{\partial^2 u_1}{\partial y^2}-\kappa J\frac{\partial u_1}{\partial x}-\kappa^2J^2u_1 \tag{4}$$

The x-momentum equation

$$\frac{\partial u_2}{\partial t}+\frac{\partial u_2^2}{\partial x}+\frac{\partial (u_3u_2)}{\partial y}+\kappa J u_1^2-\kappa J u_2^2=-p_x+\frac{\partial^2 u_2}{\partial x^2}+\frac{\partial^2 u_2}{\partial y^2}-\kappa J\frac{\partial u_2}{\partial x}-\kappa^2J^2u_2 \tag{5}$$

The y-momentum equation

$$\frac{\partial u_3}{\partial t}+\frac{\partial (u_2u_3)}{\partial x}+\frac{\partial u_3^2}{\partial y}-\kappa J u_2u_3=-p_y+\frac{\partial^2 u_3}{\partial x^2}+\frac{\partial^2 u_3}{\partial y^2}-\kappa J\frac{\partial u_3}{\partial x} \tag{6}$$

The symmetry of the flow along the x-axis permits the solution domain to be restricted to the upper half of the cross-section. Therefore, the associated boundary conditions are

$$u_1=u_2=u_3=0 \text{ at the wall},\quad \frac{\partial u_2}{\partial y}=\frac{\partial u_1}{\partial y}=u_3=0 \text{ along the } x\text{-axis},\ y=0 \tag{7}$$

Another important quantity is the non-dimensional product of the friction factor f and the Reynolds number Re which is given by the expression

$$fRe = \frac{-1}{2U_{\mathrm{av}}} \frac{\partial p^{\mathrm{a}}}{\partial s}, \quad U_{\mathrm{av}} \equiv u_{1\mathrm{m}} = \frac{2}{S} \int_0^{1/2} \int_{-1/2}^{1/2} u_1 \, \mathrm{d}x \, \mathrm{d}y \tag{8}$$

where $S = a^2$ is the cross-section urea, $u_{1\mathrm{m}}$ is the dimensionless average axial velocity, $Re = u_{1\mathrm{m}} D_h/v = U_{\mathrm{av}}$ is the Reynolds number and $D_{\mathrm{h}} = a$ is the hydraulic diameter.

The quasi-linear, second-order partial differential equations are discretized and solved numerically by a time marching algorithm, calculating the velocity components and pressure at the $n+1$ time level from their corresponding values at the n level. The algorithm consists of two steps. At the first step, the axial momentum equation (4) will be solved alone, iteratively with respect to the axial velocity u_1, for prescribed values of the axial pressure gradient $p^{\mathrm{a}}_{s'}$ and curvature κ, using zero transverse velocities u_2 and u_3. The obtained solution will be used as the u_1 profile at the $n=1$ time level. At the second step, Equations (5) and (6) will be solved with an additional set of equations for the determination of u_2, u_3 and pressure p at the $n+1$ time level, using the proposed CVP computational method. The obtained values are inserted successively into Equation (4) and the system of the involved equations for the calculation of the improved u_1, u_2, u_3 and p at the $n+1$ level and the overall iteration of the system is repeated until convergence is achieved.

The detailed solutions of Equations (3)–(6) with our proposed CVP method and the PLEM scheme, which is a variation of the pressure linked equations, are described in the next section.

3. CALCULATION PROCEDURES

3.1. The CVP method

In the CVP method the system of Equations (3)–(6) under the boundary conditions (7) will be solved with a time iterative procedure where, for simplicity, the system of Equations (4)–(6) is linearized by lagging the coefficients. At first, for a given axial pressure gradient $p^{\mathrm{a}}_s = \partial p^{\mathrm{a}}/\partial s$ and curvature κ, the best initial profile for the axial velocity u_1 is obtained solving Equation (4) alone, with the ADI method, using zero transverse velocities u_2 and u_3. Then, knowing the axial velocity u_1 at the $n=1$ level, the profile u_1^{n+1} at each successive time level $n+1$ is calculated, for the given values of the parameters κ and $p^{\mathrm{a}}_s = \partial p^{\mathrm{a}}/\partial s$, from Equation (4) which is written as

$$\frac{\partial u_1^{n+1}}{\partial t} + A_1(u_1^{n+1}) - \nabla_{\mathrm{c}}^2 u_1^{n+1} - \kappa J u_3^n u_1^{n+1} + \kappa J \frac{\partial u_1^{n+1}}{\partial x} + \kappa^2 J^2 u_1^{n+1} = -J p^{\mathrm{a}}_{\mathrm{s}} \tag{9}$$

$$A_1(u_1^{n+1}) = \frac{\partial (u_2^n u_1^{n+1})}{\partial x} + \frac{\partial (u_3^n u_1^{n+1})}{\partial y}$$

where $\partial u_1^{n+1}/\partial t = (u_1^{n+1} - u_1^n)/\Delta t$ and $\nabla_{\mathrm{c}}^2 = \partial^2/\partial x^2 + \partial^2/\partial y^2$.

Defining $p_2 \equiv p_x$, $p_3 \equiv p_y$ the corresponding transverse linearized momentum equations take, respectively, the forms

$$\frac{\partial u_2^{n+1}}{\partial t} + A_2(u_2^{n+1}) - \nabla_{\mathrm{c}}^2 u_2^{n+1} + KJ \frac{\partial u_2^{n+1}}{\partial x} + KJ(u_1^n)^2 = -p_2^{n+1} \tag{10a}$$

where

$$A_2(u_2^{n+1}) = \frac{\partial(u_2^n u_2^{n+1})}{\partial x} + \frac{\partial(u_3^n u_2^{n+1})}{\partial y} - KJ\, u_2^n u_2^{n+1} + K^2 J^2 u_2^{n+1}$$

$$\frac{\partial u_3^{n+1}}{\partial t} + A_3(u_3^{n+1}) - \nabla_c^2 u_3^{n+1} + KJ\, \frac{\partial u_3^{n+1}}{\partial x} = -p_3^{n+1} \tag{10b}$$

where

$$A_3(u_3^{n+1}) = \frac{\partial(u_2^n u_3^{n+1})}{\partial x} + \frac{\partial(u_3^n u_3^{n+1})}{\partial y} - KJ u_2^n u_3^{n+1}$$

Substituting the relations

$$\begin{aligned} u_2^{n+1} &= u_2^* + \delta u_2, \quad p^{n+1} = p^n + \delta p \\ u_3^{n+1} &= u_3^* + \delta u_3, \quad p_b^{n+1} = p_b^n + \delta p_p, \quad b = 2,3 \end{aligned} \tag{11}$$

into (9), (10a) and (10b) the equations are splitted in two parts, the system

$$\frac{\partial u_2^*}{\partial t} + A_2(u_2^*) - \nabla_c^2 u_2^* + \kappa J\, \frac{\partial u_2^*}{\partial x} + \kappa J (u_1^n)^2 = -p_x^n \tag{12}$$

$$\frac{\partial u_3^*}{\partial t} + A_3(u_3^*) - \nabla_c^2 u_3^* + \kappa J \frac{\partial u_3^*}{\partial x} = -p_y^n \tag{13}$$

where

$$A_2(u_2^*) = \frac{\partial(u_2^n u_2^*)}{\partial x} + \frac{\partial(u_3^n u_2^*)}{\partial y} - \kappa J u_2^n u_2^* + K^2 J^2 u_2^* \tag{14a}$$

$$A_3(u_3^*) = \frac{\partial(u_2^n u_3^*)}{\partial x} + \frac{\partial(u_3^n u_3^*)}{\partial y} - \kappa J u_2^n u_3^* \tag{14b}$$

and the pressure gradient correction equations, which defining $f_2 = \delta p_x$, $f_3 = \delta p_y$, take the form

$$\frac{\partial \delta u_2}{\partial t} + A_2(\delta u_2) - \nabla_c^2 \delta u_2 + \kappa J\, \frac{\partial \delta u_2}{\partial x} = -\delta p_x = -f_2 \tag{15}$$

$$\frac{\partial \delta u_3}{\partial t} + A_3(\delta u_3) - \nabla_c^2 \delta u_3 + \kappa J \frac{\partial \delta u_3}{\partial x} = -\delta p_y = -f_3 \tag{16}$$

The terms $A_2(\delta u_2)$ and $A_3(\delta u_3)$ are obtained from (14a) and (14b) replacing u_2^* and u_3^* by δu_2 and δu_3, respectively.

Solving Equations (12) and (13) for known values of the terms p_x^n and p_y^n we obtain the estimated components u_2^* and u_3^* which do not satisfy the continuity equation (3).

In our CVP method, for the determination of the corrections δu_2 and δu_3 a system of variational equations is required which is constructed as follows. At first the continuity variational equation is obtained from (3) using (10) so that

$$\frac{\partial \delta u_2}{\partial x} + \frac{\partial \delta u_3}{\partial y} - \kappa J \delta u_2 = G \quad \text{where } G = -\left(\frac{\partial u_2^*}{\partial x} + \frac{\partial u_3^*}{\partial y}\right) + \kappa J u_2^* \tag{17}$$

Secondly differentiating (16) and (15) with respect to x and y, respectively, and subtracting the produced equations, the vorticity variational equation is obtained. Substituting into the produced equation, the vorticity correction $\delta\boldsymbol{\omega}$ defined by

$$\boldsymbol{\nabla} \times \delta\mathbf{U} = \delta\boldsymbol{\omega} = \delta\omega\mathbf{k}, \quad \delta\omega = \frac{\partial \delta u_3}{\partial x} - \frac{\partial \delta u_2}{\partial y} \tag{18}$$

and neglecting the terms depending on κ^2 and the quantity $(\partial A_3(\delta u_3)/\partial x - \partial A_2(\delta u_2)/\partial y)$ as particularly small, the vorticity variational equation is obtained which takes the form

$$\frac{\partial \delta\omega}{\partial t} - \nabla_c^2 \delta\omega + \kappa J \frac{\partial \delta\omega}{\partial x} = 0 \quad \text{or} \quad \nabla_c^2 \delta\omega - KJ \frac{\partial \delta\omega}{\partial x} - \frac{\delta\omega}{\Delta t} = 0 \tag{19}$$

considering that $\partial\delta\omega/\partial t = (\delta\omega^{n+1} - \delta\omega^n)/\Delta t = \delta\omega/\Delta t$ where $\delta\omega^n = 0$. Equation (19) is solved with the boundary condition

$$\delta\omega_c = \left(\frac{\partial \delta u_3}{\partial x} - \frac{\partial \delta u_2}{\partial y} \right)\Bigg|_c$$

where c is the contour enclosing the cross-section area. Solving the system of Equations (17) and (18) in conjunction with Equation (19) we could evaluate the corrections δu_2 and δu_3. However, the solutions of the first-order partial differential equations cannot satisfy all the boundary conditions $\delta u_2 = \delta u_3 = 0$ at the walls, because in that case the equations should be over-determined. For dealing with this problem we can use a theorem which has been proved by us in References [18, 19] and instead of solving (17) and (18), we can solve an equivalent system of second order partial differential equations. These equations are obtained differentiating (17) with respect to x and y and expressing the first and mixed derivatives, using (18), in terms of $\delta\omega$.

Hence in our method instead of (17) and (18) we solve the equations

$$\nabla_c^2 \delta u_3 - \kappa J \frac{\partial \delta u_3}{\partial x} = \frac{\partial G}{\partial y} + \frac{\partial \delta\omega}{\partial x} - \kappa J \delta\omega \tag{20}$$

$$\nabla_c^2 \delta u_2 - \kappa \frac{\partial (J \delta u_2)}{\partial x} = \frac{\partial G}{\partial x} - \frac{\partial \delta\omega}{\partial y} \tag{21}$$

under the boundary conditions

$$\begin{aligned} \delta u_2 &= \delta u_3 = 0 \quad \text{at the wall} \\ \frac{\partial \delta u_2}{\partial y} &= \delta u_3 = 0 \quad \text{at the } x\text{-axis}, y = 0 \end{aligned} \tag{22}$$

For the restriction of the numerical violation of the theoretical equations (17) and (18), calculated using the solutions of equations (20) and (21), we apply the following technique. At first solving (20) we obtain δu_3. Consequently, calculating the second-order derivative of δu_2 with respect to its non-parallel co-ordinate y from (18) and substituting its value into (21), we obtain the Poisson equation

$$\frac{\partial^2 \delta u_2}{\partial x^2} - \kappa \frac{\partial (J \delta u_2)}{\partial x} = \frac{\partial G}{\partial x} - \frac{\partial \delta\omega}{\partial y} - Q \quad \text{where } Q = \frac{\partial^2 \delta u_2}{\partial y^2} = \frac{\partial^2 \delta u_3}{\partial y \partial x} - \frac{\partial \delta\omega}{\partial y} \tag{23}$$

under the boundary conditions (22).

Substituting δu_2 and δu_3 into (15) and (16), the pressure gradient correction functions f_2 and f_3, are evaluated and the pressure correction δp is obtained solving the pressure variational equation

$$\nabla_c^2 \delta p = \sum_{b=2}^{3} \frac{\partial \delta p_b}{\partial x_b} = \sum_{b=2}^{3} \frac{\partial f_b}{\partial x_b} \quad \text{where} \quad \frac{\partial \delta p}{\partial x} = \frac{\partial \delta p}{\partial y} = 0 \quad \begin{matrix} \text{at the wall and} \\ \text{the } x\text{-axis, } y=0 \end{matrix} \tag{24}$$

Substituting δu_2, δu_3, δp and the calculated derivatives δp_x and δp_y into (11) we obtain at the $n+1$ time level the required quantities, which satisfy also the continuity equation. Substituting $u_1^{n+1}, u_2^{n+1}, u_3^{n+1}$ and p_x^{n+1}, p_y^{n+1} at the place of the corresponding variables at the time level n, the iteration is repeated until convergence is achieved.

We consider three versions of the method denoted CVP(i), CVP(ic) and CVP(r). The CVP(i) version concerns the irrotational correction of the velocity components so that $\delta\omega = 0$. In this case the algorithm is simplified as Equation (19) is not involved, while Equations (20)–(23) are simplified. In this version the convection and diffusion terms are also neglected from the pressure gradient correction equations (15) and (16). The CVP(ic) version is also an irrotational version like the CVP(i); however, the diffusion terms in Equations (15) and (16) are taken into account. The CVP(r) version concerns the rotational correction of the velocity components, $\delta\omega \neq 0$. In this case also only the diffusion terms in Equations (15) and (16) are taken into account.

3.2. *Computational algorithms of the CVP method*

The computational algorithms of the irrotational CVP(i), CVP(ic) and the rotational CVP(r) versions differ substantially. In the irrotational algorithm Equation (19) and the terms of Equations (20)–(23) depending on $\delta\omega$ and its derivatives are omitted. Thus, at each $n+1$ time level only the two Poisson equations (20) and (23) are solved for the determination of δu_2 and δu_3.

In the rotational algorithm, the solution of (19) for $\delta\omega$ depends on the boundary, from the values of the partial derivatives of δu_2 and δu_3 which initially are unknown. Thus, at each time level $n+1$, the system of the three Poisson equations (19), (20) and (23) is solved with an internal iterative procedure setting initially $\delta\omega_c = 0$ at the boundary, until convergence is achieved.

It is noted that before starting the iterative procedure, the initial parabolic profile for the axial velocity u_1 at $n=1$, is obtained solving Equation (9) alone, for the given values of the parameters κ and p_s^a, with $u_2 = u_3 = 0$, using the ADI method. Then knowing the axial velocity u_1 at the $n=1$ level, the profile u_1^{n+1} at each successive time level $n+1$ is calculated from Equation (9), taking into account the calculated transverse velocities.

The CVP-methodology is summarized at each $n+1$ time level as follows:

1. The axial component u_1^{n+1} is obtained from (9) for a given p_s^a and the first estimations for the transverse components u_2^* and u_3^* are obtained from (12) and (13) for known values of p_x^n, p_y^n, u_2^n, u_3^n and u_1^n. For $n=1$ we define $p_x = p_y = 0$, $u_2 = u_3 = 0$, while u_1 is already known. Equations (9), (12) and (13) are solved with the two-dimensional ADI method.
2. At each $n+1$ level, in the CVP(r) version, an internal iterative procedure is applied with index $m = 0, 1, 2, \ldots$. For the calculation of $\delta\omega$, from (19), its value on the boundary is needed. Initially at $m=1$ the derivatives of δu_2 and δu_3 are not known so we define

$\delta\omega_c = 0$. For $m = 2, 3 \ldots, \delta\omega_c$ is calculated from the known values of δu_2 and δu_3. In the irrotational case $\delta\omega = 0$, thus Equation (19) and the internal iteration procedure are omitted.

3. The corrections δu_3 and δu_2 are obtained from (20) and (23). For $\delta\omega \neq 0$ we go back to step 2 and the internal procedure is repeated until convergence is achieved.
4. The functions $f_1 = \delta p_x$, $f_2 = \delta p_y$ are obtained from (15) and (16).
5. The correction δp is obtained from (24).

The values of $u_2^{n+1}, u_3^{n+1}, p^{n+1}\, p_b^{n+1}$ $(b = x, y)$ are provided by (11). Inserting these quantities into equations or step (1) the time iteration procedure is repeated.

3.3. PLEM-method

This methodology is a variation of the method developed by Hirt *et al.* [20] within the framework of MAC formalism, however, applying a non-staggered grid. In this method the momentum equations are linearized by lagging the coefficients and the axial velocity u_1^{n+1} at the time level $n+1$ is calculated for a known p_s^{a} by Equation (9). Using relations (11), at each time level $n+1$, the first estimated values for the transverse velocities u_2^*, u_3^* are evaluated solving Equations (12) and (13) for known values of p_x^n and p_y^n. Then the corrections δu_2 and δu_3 satisfy the approximated equations.

$$\frac{\partial \delta u_2}{\partial t} \approx \frac{\delta u_2}{\Delta t} = -\frac{\partial \delta p}{\partial t}, \quad \frac{\partial \delta u_3}{\partial t} \approx \frac{\delta u_3}{\Delta t} = -\frac{\partial \delta p}{\partial y} \tag{25a}$$

or

$$u_2^{n+1} = u_2^* - \Delta t \frac{\partial \delta p}{\partial x}, \quad u_3^{n+1} = u_3^* - \Delta t \frac{\partial \delta p}{\partial y} \tag{25b}$$

Substituting (25b) into the continuity equation (3), the equation for the pressure correction δp is obtained

$$\nabla_{\mathrm{c}}^2 \delta p - \kappa J \frac{\partial \delta p}{\partial x} = \frac{1}{\Delta t}\left(\frac{\partial u_2^*}{\partial x} + \frac{\partial u_3^*}{\partial y} - \kappa J u_2^*\right) \tag{26}$$

subjected to the boundary condition $\nabla p \cdot \mathbf{n} =$ at the wall and the symmetry x-axis, $y = 0$. Using the solution of (26), the pressure is given by $p^{n+1} = p^n + \delta p$ and the velocity components u_2^{n+1} and u_3^{n+1} are determined by (25b). Inserting these values in place of those at the nth time level, we continue the iterative procedure.

4. NUMERICAL DISCRETIZATION AND ACCURACY

For the solution of the equations within the finite-difference formulation a collocated uniform grid is used, where velocity components and pressure are defined at the same nodes. Thus if the required variables are represented by the dummy variable Φ, at each grid point t_n, x_i, y_j $(n, I, j = 1, 2, \ldots, N, I, J)$ they are denoted as $\Phi_{i,j,k}^n$ The time derivatives are approximated by two-point backward differences while the space derivatives are approximated by three-point central differences at the internal nodes of the flow region and one-sided three-point formulas, of second-order of accuracy, at the boundary nodes. It must be emphasized that the functions

G, Q, f_2, f_3 must be evaluated as functions at all interior and boundary nodes before their use in Equations (17) and (20)–(24). In the CVP and PLEM methods Equations (9), (12) and (13) are solved using the ADI iterative method. The involved Poisson equations are solved with the successive overrelaxation (SOR) iterative algorithm.

4.1. Criteria for convergence

The ADI algorithms have been solved with a time step Δt which satisfies the condition

$$\Delta t \leqslant \frac{1}{6}\frac{(\Delta x^2 + \Delta y^2)}{2} \tag{27}$$

for ensuring that the numerical results should not be affected by the doubling or tripling of Δt by more than 1%.

The applied iterative procedure is repeated until the following convergence criterion is satisfied.

$$\left[\frac{1}{J-I}\sum_{i,j=1}^{I,J}\frac{(\Phi^{n+1}-\Phi^n)^2}{(\Phi^{n+1})^2}\right]^{1/2} < e_1 = 5\times 10^{-5} \tag{28}$$

where I,J are the grid nodes along the x- and y-axis, respectively. Φ stands for u_1, u_2 and u_3. In the rotational version CVP(r), at each $n+1$ level, the internal iteration procedure is repeated until the following convergence criterion is satisfied:

$$\left[\left(\sum_{i,j=1}^{I,J}\delta w\right)^{n+1} - \left(\sum_{i,j=1}^{I,J}\delta w\right)^{m}\right] \Bigg/ \left(\sum_{i,j=1}^{I,J}\delta w\right)^{m+1} < e_2 \tag{29}$$

where δw stands for δu_2 and δu_3. The optimal values for e_2 are of the order of 0.5. The iterations do not exceed the numbers $m=2$ or 3 except for the first few time iterations.

Each of the involved Poisson equations is solved with the SOR iterative algorithm, using values around the optimum relaxation parameter $\lambda = 2/(1+\sqrt{1-\lambda_0^2})$ where $\lambda_0 = \{\Delta y^2\cos(\pi/q_1) + \Delta x^2\sin(\pi/q_2)\}/(\Delta x^2+\Delta y^2)$ with $q_1 = I-1$ and $q_2 = J-1$. The SOR algorithms were repeated until convergence criterions similar to that of (28) were satisfied with Φ standing for $\delta\omega, \delta u_2, \delta u_3$ and δp. However, the velocity and pressure Poisson equations were solved with $e_1 = 0.05$ and 0.5, respectively.).

It is clear that the reduced accuracy of the Poisson equations and of the internal iteration, does not affect the accuracy of the method which is governed by criterion (28), but reduces drastically the time of convergence.

The convergence criterion for the PLEM scheme is given by (28).

4.2. Numerical accuracy

The effect of the grid size on the results for the product $f_c Re$, obtained with the CVP(i), CVP(ic), CVP(r) and PLEM methods, for flows with Dean number $De \approx 55$, $p_s^a = -19.000$ and curvature $\kappa = 0.01$, is shown in Table I. Similar results are presented in Table II for $De \approx 189$, $p_s^a = -20.000$ and $\kappa = 0.1$. It is observed that for $De \approx 55$, the divergence of the values of fRe, obtained using the grids 21×11 and 101×51, is about 0.105% in the CVP(i)

Table I. Results for fRe obtained by CVP(i), CVP(ic), CVP(r) and PLEM methods, for flows with $De \approx 55$ ($p_s^a = -19\,000$, $\kappa = 0.01$) and various grids.

Method	CVP(i)	CVP(ic)	CVP(r)	PLEM
Grid	fRe	fRe	fRe	fRe
21×11	17.2252	17.2811	—	17.3741
41×21	17.2246	17.2783	17.2612	17.2314
51×26	17.2207	17.2709	17.2546	17.2126
61×31	17.2055	17.2583	17.2313	17.1923
81×41	17.2072	17.2281	17.2157	17.1568
101×51	17.2071	17.2388	17.1938	17.1589

Table II. Results for fRe obtained by CVP(i), CVP(ic) and PLEM methods, for flows with $De \approx 189$ ($p_s^a = -20\,000$, $\kappa = 0.1$) and various grids.

Method	CVP(i)	CVP(ic)	PLEM
Grid	fRe	fRe	fRe
21×11	24.2143	24.1968	25.8000
41×21	25.0023	25.0340	25.2550
51×26	25.0810	25.1222	25.1800
61×31	25.1164	25.1646	25.1384
81×41	25.1361	25.1848	25.0910
101×51	25.1334	25.1794	25.0720

version, 0.245% in the CVP(ic) version, 0.39% in the CVP(r) version and 1.254% in the PLEM method. The corresponding divergence for the results obtained with $De \approx 189$ is 3.67% in the CVP(i) version, 3.93% in the CVP(ic) version and 2.8% in the PLEM method. In conclusion the effect of the grid size although insignificant for small Dean numbers, increases as the Dean number increases. In general, the effect of the grid size on the results obtained by the three versions of the CVP method, for the same parametric values, is marginal. The increase of the grid size increases the accuracy of the numerical results and improves the conditions for the convergence of the numerical method. The decrease of the steps Δx and Δy results to the decrease of the grid Peclet numbers $u_2^* \Delta x$, $u_3^* \Delta t$ to values lower than the critical value $Pe_0 = 2$ at each grid point. Thus, in the diagonal systems of the algebraic equations representing the discretized Navier–Stokes equations, the condition of diagonal dominance is satisfied, eliminating spurious oscillations from the solutions.

The differences between the results obtained by the CVP versions for fRe are small. Thus for $De \approx 55$ and $\kappa = 0.01$, the difference of the results obtained with the CVP(i) and CVP(ic) schemes is about 0.183%, for those obtained with CVP(i) and CVP(r) is about 0.061% and for those obtained with CVP(ic) and CVP(r) is about 0.134%. Similar results are obtained when the curvature is $\kappa = 0.1$. When the convection and diffusion terms in the pressure correction equations are taken into account by the three CVP versions, the observed differences of the results for fRe are smaller than $\pm 0.2\%$. In Figures 2 and 3 the effect of the grid size on the total number of time iterations and on the required CPU time, using a Pentium III 800MHz, are shown, respectively. Hereafter, the presented results have been obtained with a grid 81×41,

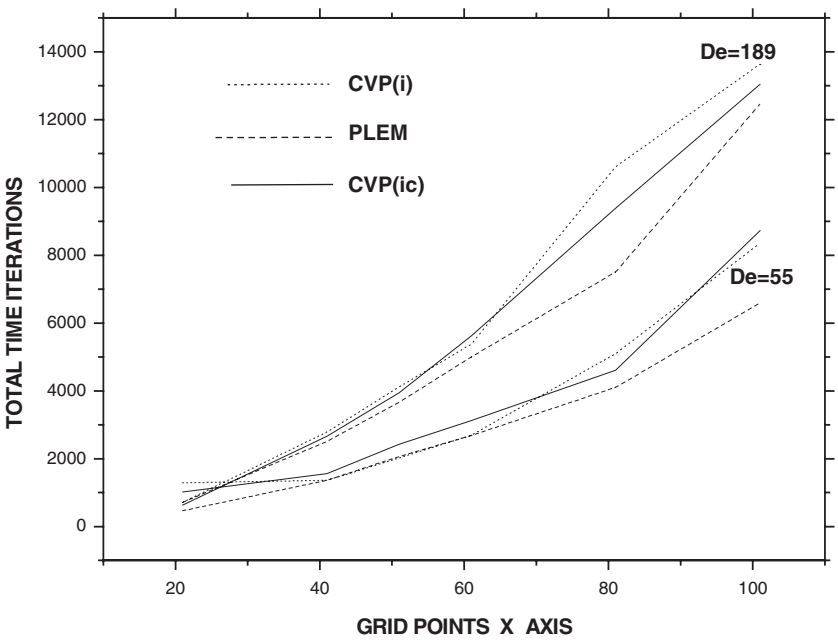

Figure 2. Dependence of time iterations for convergence on the grid size for the CVP and PLEM methods.

except if it is defined otherwise. From Figures 2 and 3 it is observed that the number of time iterations and the CPU time decrease when the diffusion terms are taken into account in the pressure correction equations.

5. RESULTS AND DISCUSSION

The CVP(i) and PLEM results for the axial velocity component u_1/U_0 along the vertical yy' $(x=0)$ axis are shown in Figure 4, for flows with Dean numbers $De=55\,189$ and $\kappa=0.1$. The differences of the results of the two methods are particularly small for the axial velocity. However, these differences increase substantially for the transverse velocity components u_2 and u_3 as the Dean number increases.

The profiles of u_2 and u_3 along the yy'-axis $(x=0)$ of symmetry for $De=55$ and 189 are shown, respectively, in Figures 5 and 6. As the Dean number increases to higher values, the velocity u_2 changes drastically, decreasing in the region $y\leqslant 0.35$ and increasing substantially for $y>0.35$. In addition, although the distribution profile of u_3 is reversed, its magnitude is much less affected by the increase of De. The observed behaviour of the transverse velocities is due to the appearance of an additional pair of vortices in the secondary flow above a critical Dean number.

In Figures 7 and 8, the profiles of the axial velocity u_1/U_a are shown with respect to the xx' and yy' axes, respectively, for various Dean numbers and are compared with those obtained

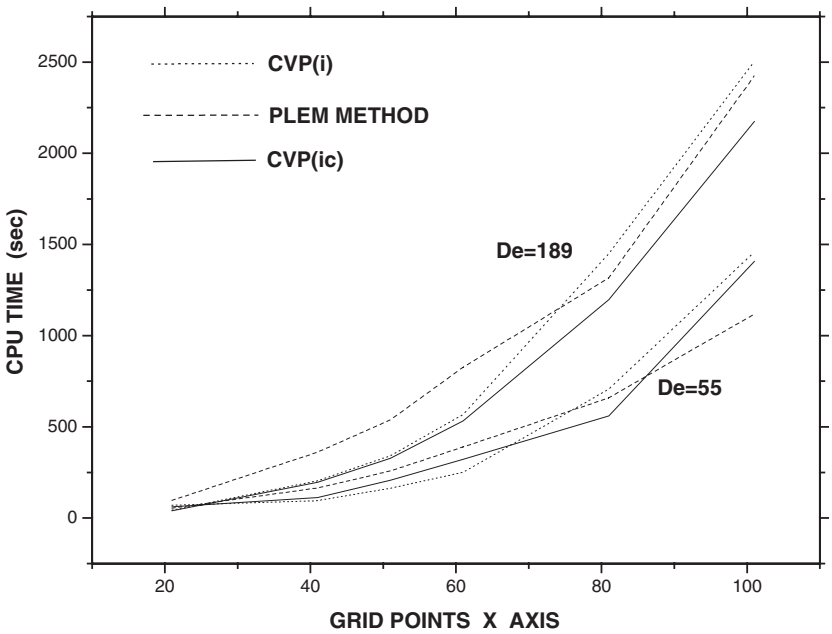

Figure 3. Dependence of the CPU time on the grid size for the CVP and PLEM methods.

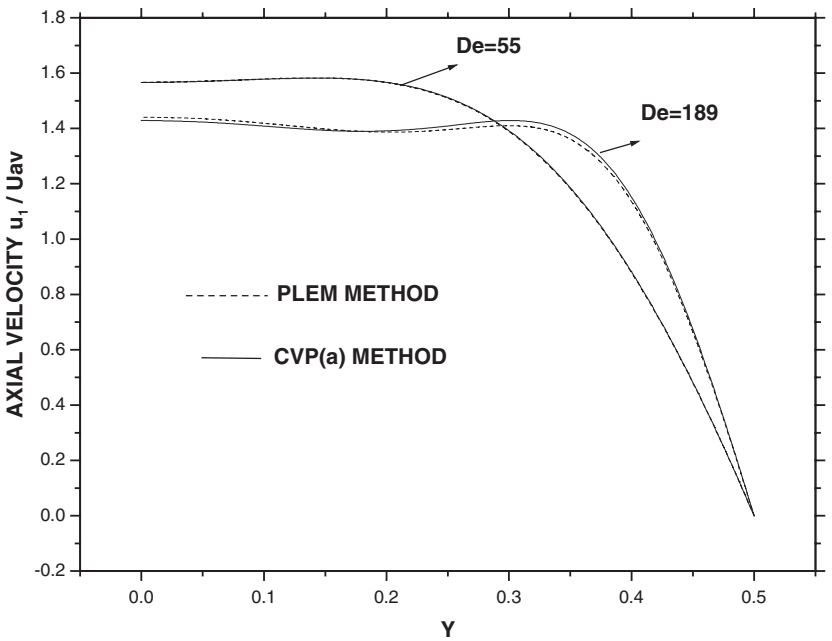

Figure 4. The u_1/U_0 profiles along the yy' $(x=0)$ axis when $\kappa=0.1$.

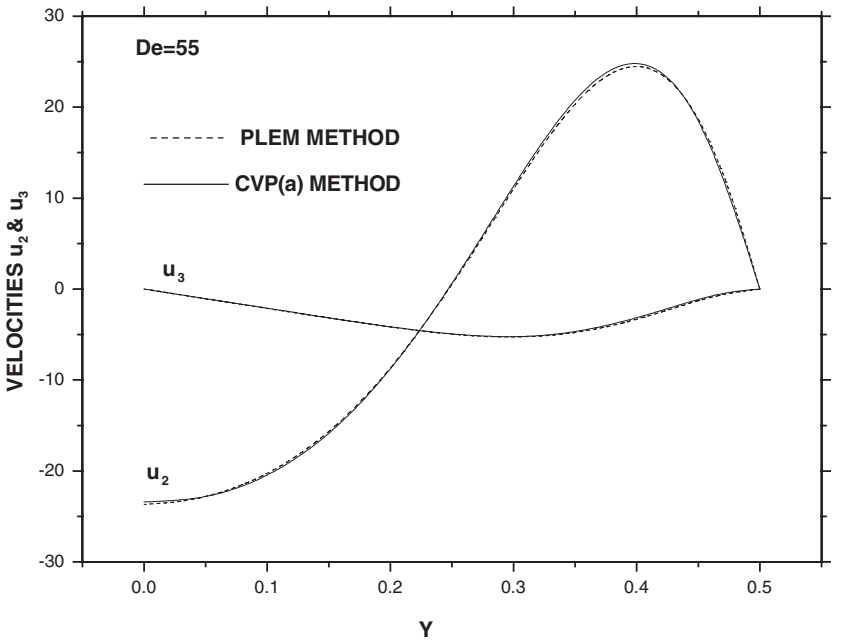

Figure 5. The u_2 and u_3 profiles along the yy' $(x=0)$ axis when $\kappa=0.1$ and $De=55$.

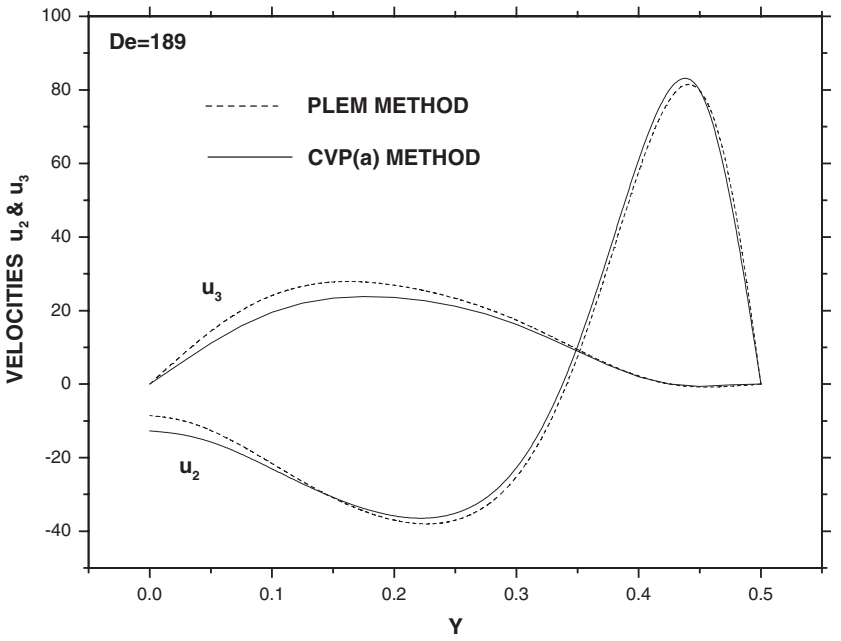

Figure 6. The u_2 and u_3 profiles along the yy' $(x=0)$ axis when $\kappa=0.1$ and $De=189$.

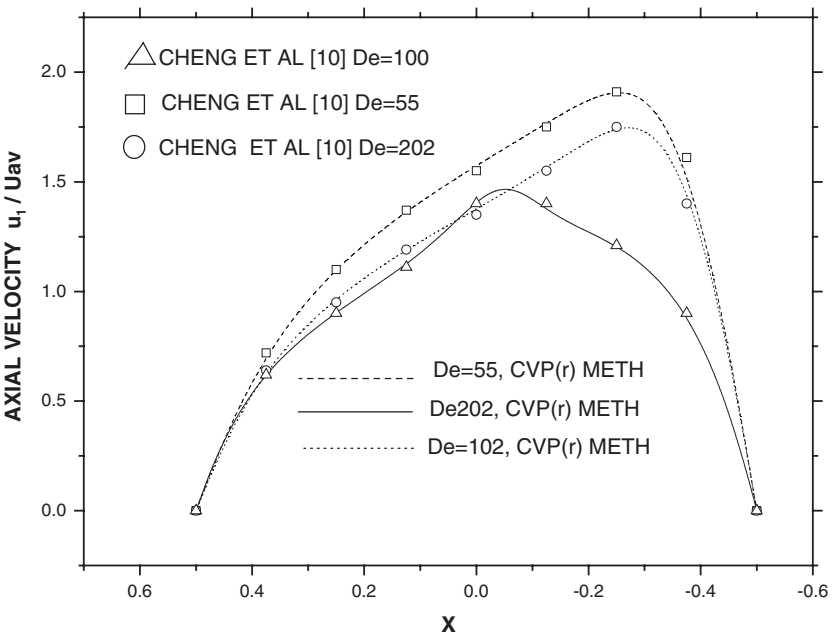

Figure 7. The u_1/U_0 profiles along the xx' $(y=0)$ axis when $\kappa=0.01$.

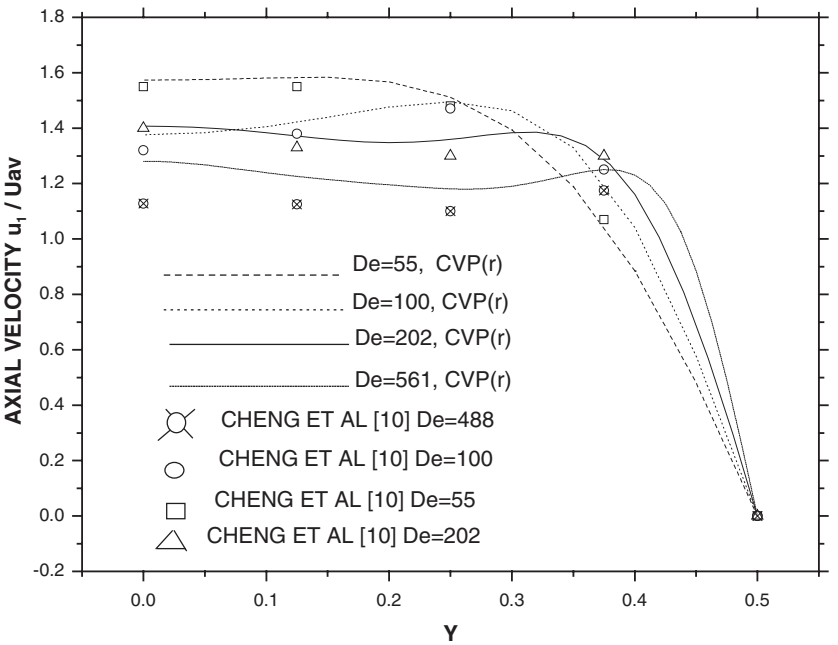

Figure 8. The u_1/U_0 profiles along the yy' $(x=0)$ axis when $\kappa=0.01$.

Table III. Values of f_c/f_s and De for various values of p_s^a when $\kappa = 0.01$, by various methods.

P_s^a	CVP(i) $f_c/f_s/De$	CVP(r) $f_c/f_s/De$	Cheng [10] $f_c/f/De$	Chen [21] $f_c/f_s/De$	Komiyama [13] $f_c/f_s/De$	Duh [16] $f_c/f_s/De$	Hwang [11] $f_c/f_s/De$	Dong [14] $f_c/f_s/De$	Bolinder [22] $f_c/f_s/De$
−19 000	1.21/ 55.15	—	1.22/ 54.8	—	1.20/ 55.4	1.21/ 55.42	1.219/	—	1.216
−30 000	1.314/ 80.26	1.306 80.69	—	—	—	—	1.323/	—	1.327
−40 000	1.383/ 101.6	1.381/ 101.7	1.41/ 100	1.38/ 101.8	1.375/ 101.8	1.37/ 103.3	1.392	1.42/ 99.1	1.41
−45 000	1.414/ 111.8	1.41/ 111.9	—	1.41/ 112	—	—	1.421	—	1.447
−50 000	1.444/ 121.8	1.441/ 121.9	—	1.44/ 122.1	—	—	1.519	—	1.48
−55 000	1.52/ 127.16	1.518/ 127.13	—	1.47/ 131.8	—	—	1.5413	—	1.498
−70 000	1.625/ 151.4	1.627/ 151.2	1.63/ 151.1	—	1.627/ 150.5	—	1.632	—	1.575
−110 000	1.83/ 211.5	1.834/ 210.8	1.91/ 202.6	1.76/ 200	1.838/ 209.5	1.78/ 218.5	1.825	1.92/ 201.4	1.75
−120 000	1.867/ 225.8	1.874/ 225	—	1.86/ 227.3	—	—	1.866	—	1.789
−200 000	2.102/ 334.4	2.119/ 331.7	—	—	2.156/ 324.6	—	2.135	—	2.076

Table IV. Values of f_c/f_s and De for various values of p_s^a when $\kappa = 0.1$, by various methods.

P_s^a	CVP(i) $f_c/f_s/De$	CVP(ic) $f_c/f_s/De$	CVP(r) $f_c/f_s/De$	Cheng [10] $f_c/f_s/De$	Hwang [11] $f_c/f_s/De$	Bolinder [22] f_c/f_s	Dong [14] $f_c/f_s/De$
−50 000	2.002/ 277.46	2.016/ 275.55	2.012/ 276.15	2.11 262.7	2.002	1.929	—
−55 000	2.047/ 298.55	2.063/ 296.3	2.058/ 297	2.15/ 283.4	2.053	1.983	—
−80 000	2.228/ 398.9	2.247/ 395.7	2.245/ 395.9	2.44/ 364.3	2.273	2.235	2.36/ 376.6
−10 000	2.345/ 437.82	2.359/ 471.1	2.369/ 469	—	2.418	2.41	—

by Cheng *et al.* [10]. The maximum value of the axial velocity u_1, which appears near the outer wall for small Dean numbers, progressively moves to the centre of the x-axis whereas its magnitude decreases as the Dean number increases. This is due to the corresponding increase of the transverse velocity components.

Denoting by f_c and f_s the friction factors corresponding to curved and straight square duct, the values of the ratio f_c/f_s and of the Dean number De are presented for various axial pressure gradients p_s^a in Table III for $\kappa = 0.01$, in Table IV for $\kappa = 0.1$ and in Table V for $\kappa = 0.25$. The average value $f_s R_e = 14.23$ for the straight square duct has been estimated by an analytical formula. The results obtained with the CVP(i), CVP(ic) and CVP(r) versions are compared with those obtained by Cheng *et al.* [10], Komyiana *et al.* [13], Hwang *et al.* [11] using the vorticity–free stream formalism, by Duh *et al.* [16] using a velocity–pressure formalism with a non-staggered mesh, by Chen *et al.* [21] using a finite element method and by Bolinder *et al.* [22] and Dong *et al.* [14] using versions of the SIMPLE method with a staggered mesh. The percentage differences between the results obtained with the CVP(i) and CVP(r) schemes are very small, i.e., of the order 0.55%. Similar differences are observed between the results of CVP(i) and CVP(ic) versions.

In Table III for $\kappa = 0.01$ and De varying from 55 to 334, the average percentage difference of the friction ratio results obtained with the CVP(i) version and those obtained by the methods of Chen, Koniyama, Duh, Hwang and Bolinder are of the order of 1.6, 0.9, 1.24, 1.19 and 2.54%, respectively. Similar differences are observed for the results obtained with the CVP(r) version. In Table IV for $\kappa = 0.1$ the average percentage differences of the friction ratio results obtained with the CVP(ic) scheme and those obtained by the methods of Bolinder and Hwang are of the order of 1.55 and 1.49%, respectively. Analogous differences are observed in Table V for $\kappa = 0.25$.

The discrepancies between our CVP results and those obtained by Chen, Duh, Komiyama and Bolinder are smaller than 3%. However, the results of all these methods, including the CVP versions, differ from the results obtained by the methods of Cheng and Dong by more than 8% and particularly for $De > 202$. The small differences between the various methods can be justified on the bases of different approximations, methodologies and grids. However, the aforementioned large differences cannot be easily understood.

Table V. Values of f_c/f_s and De for various values of p_s^a when $\kappa = 0.25$, by various methods.

P_s^a	CVP(a) $f_c/f_s/De$	CVP(b) $f_c/f_s/De$	CVP (c) $f_c/f_s/De$	Hwang [11] $f_c/f_s/De$	Bolinder [22] f_c/f_s	Duh [16] $f_c/f_s/De$	Dong [14] $f_c/f_s/De$	Cheng [10] $f_c/f_s/De$
−25 000	1.90/	—	1.91/	1.881	1.803	1.89/	2.09/	2.04/
	231.15		230.45			233.4	211.5	214.8
−30 000	1.987/	—	1.996/	1.971	1.896	—	—	2.18/
	452.08		264.08					241.2
−60 000	2.332/	—	2.35/	2.377	2.36	—	—	2.55/
	452.08		448.7					411.9
−70 000	2.418/	2.423/	2.438/	2.483	2.49	—	—	—
	508.66	507.65	504.35					
−90 000	2.575/	2.579/	—	2.666	2.71	—	3.02/	3.04/
	614	613					523.7	520.2
−100 000	2.643/	2.648/	—	2.75	2.811	—	—	—
	664.7	663.56						

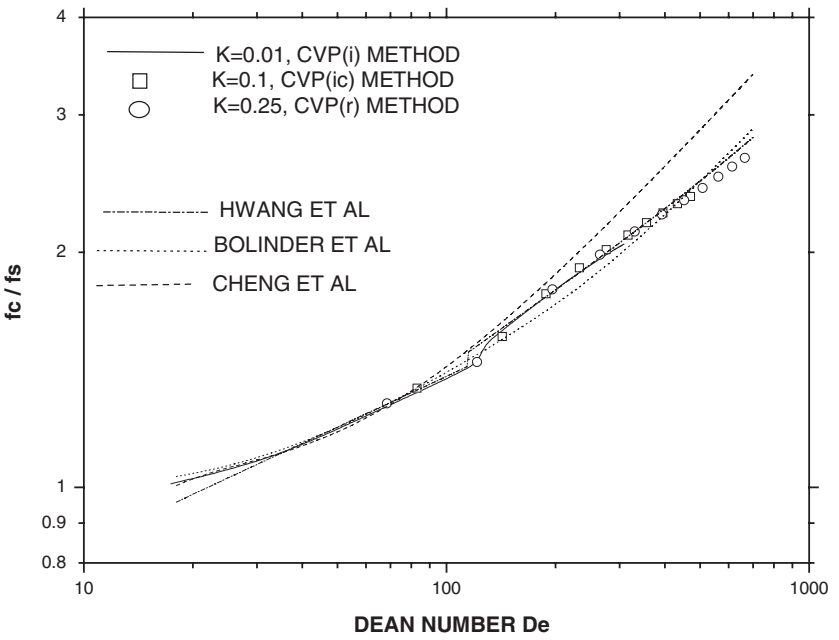

Figure 9. The friction ratio f_c/f_s versus the Dean number.

As the axial pressure gradient p_s^a decreases from -5×10^4 to -10×10^4 the ratio f_c/f_s increases about 27% when $\kappa=0.01$, 17% when $\kappa=0.1$ and 22% when $\kappa=0.25$. The clear effect of the curvature on the flow can be understood for a given value of p_s^a. For instance for $p_s^a=-55.000$, as κ increases from 0.01 to 0.1 and subsequently to $\kappa=0.25$, the value of f_c/f_s increases, respectively, about 34.7 and 7.5% and similarly the Dean number De increases, respectively, about 134.8 and 51.5%.

The variation of the friction factor ratio f_c/f_s with respect to the Dean number De is shown in Figure 9 for $\kappa=0.01$, 0.1, 0.25. It is observed that the curves present a slightly steep increase in the range of Dean numbers 110–120. This is due to the presence of an additional counterrotating pair of vortices which appears near the central part of the outer wall as it is shown in Figures 10(a) and 10(b) for flows with $\kappa=0.1$ and $De=88\,188$. The appearance of the second pair of vortices is due to the balance between the centrifugal forces and the action of the pressure gradient across the x-direction. However, the appearance or not of additional vortices depends on the instability between the aforementioned forces. The predicted values by various methods for the critical Dean number De_c, above which a second pair of vortices appears in the secondary flow, are shown in Table VI. The CVP method predicts a value $De_c\approx118$ which does not depend on the curvature. It seems that the critical value De_c, above which the flow solutions bifurcate depends strongly on the applied numerical methodology, the imposition or not of boundary conditions on the symmetry-axis, separating the upper from the lower part of the cross-section and the kind of the studied flow i.e., the fully developed or the developing flow. The distributions of pressure for flows

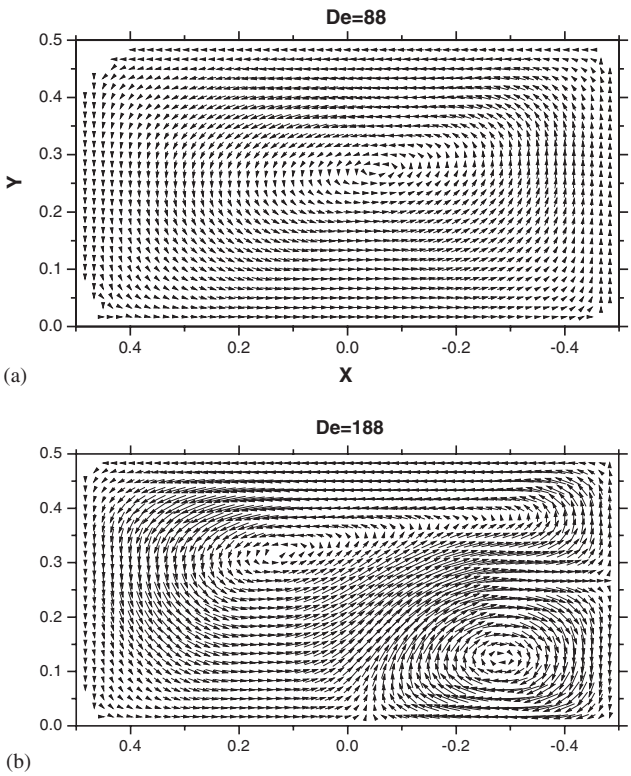

Figure 10. Effect of the Dean number on the secondary flow for $\kappa = 0.1$.

Table VI. Critical values of Dean number predicted by various methods, above which a second pair of vorticies appears.

Critical Dean number De_c	Methods
202	Cheng *et al.* [10]
113.75	Hwang and Chao [11]
125	Duh and Shih [16]
133.9	Chen and Jan [21]
124	Kamiyama *et al.* [13]
152	Joseph *et al.* [24]
125	Ghia *et al.* [23]
130	Bolinder and Sunden [22]
118	Present, CVP Method

with $\kappa = 0.1$ and $De = 140\,317$ are shown in Figure 11. Near the outer wall and the xx'-axis ($y = 0$) of symmetry the appearance of the second pair of vortices deforms the pressure distribution.

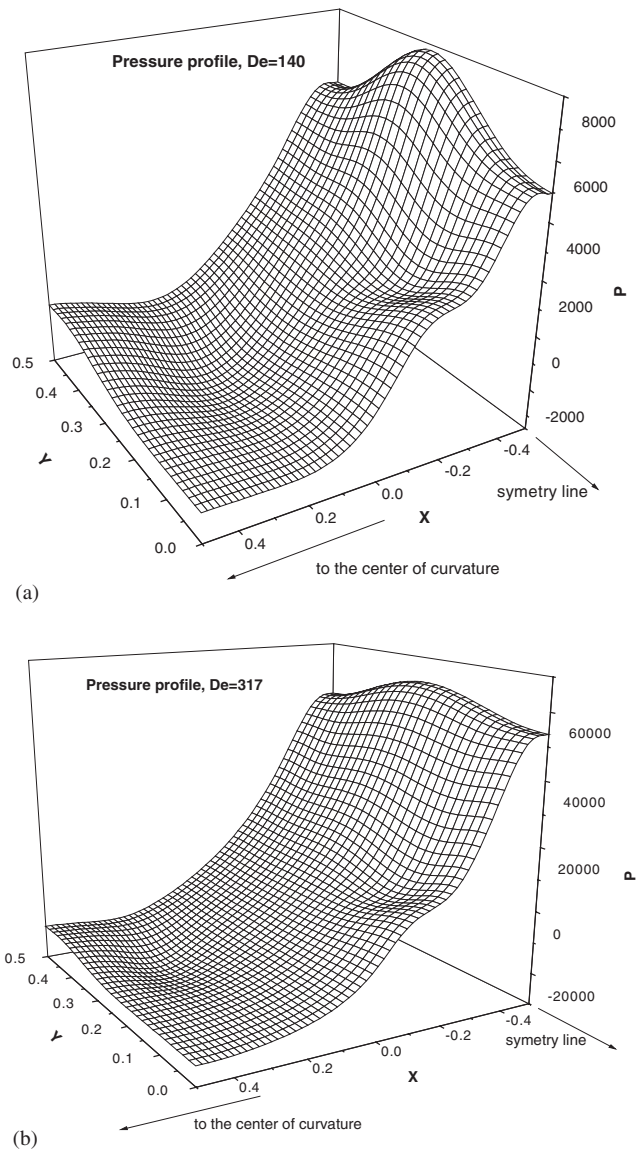

Figure 11. Transverse pressure profiles for $\kappa = 0.1$.

6. CONCLUDING REMARKS

The fully developed laminar incompressible flow is approached successfully by the new CVP method which is more easily applicable to complex internal flows, using a co-location grid without the introduction of spurious oscillations in the solutions. The method using primitive variables involves the vorticity variational equation which is much easier to obtain than the vorticity equation and particularly in complex geometries.

The analysis reveals an additional pair of secondary vortices for Dean number $De = 120$. Within the scope of the present investigation it was found that the secondary vortices disappear or appear in a wide region of Dean numbers because of the instabilities of the acting forces on the fluid. At much higher Dean numbers the additional vortices disappear.

The friction factor increases as the Dean number or the curvature κ increases.

REFERENCES

1. Dean WR. The stream line motion of fluid in a curved pipe. *Philosophical Magazine* 1928; **5**:673–695.
2. McConaloque DJ, Srivastava RS. Motion of fluid in a curved tube. *Proceedings of the Royal Society of London* 1968; **307**:37–53.
3. Greenspan D. Secondary flow in a curved tube. *Journal of Fluid Mechanics* 1973; **57**:167–176.
4. Srivastava RS. On the motion of the fluid in a curved pipe of elliptical cross-section. *Zeitschrift fur Angewandte Mathematik und Physik* 1980; **31**:297–303.
5. Topakoglu HC, Ebadian MA. Viscous laminar flow in a curved pipe of elliptical cross section. *Journal of Fluid Mechanics* 1987; **184**:571–580.
6. Mori Y, Uchida Y, Ukon T. Forced convective heat transfer in a curved channel with square cross section. *International Journal of Heat and Mass Transfer* 1971; **14**:1785–1805.
7. Mori Y, Nakayama W. Study on forced convective heat transfer in curved pipes. *International Journal of Heat and Mass Transfer* 1965; **8**:67–82.
8. Ito H. Theoretical and experimental investigation concerning the flow through curved pipes. *Memoirs of the Institute for High Speed Mechanics*, *Tohoka University* 1959; **14**:137–172.
9. Balejova M, Cakrt J, Mic V. Heat transfer for laminar flow in curved pipes with uniform wall heat flux. *Acta Technica* 1977; **2**:183–195.
10. Cheng KC, Lin RC, Ou JW. Fully developed laminar flow in curved rectangular channels. *ASME Journal of Fluids Engineering* 1976; **98**:41–48.
11. Hwang GJ, Chao CH. Forced laminal convection in a curved isothermal duct. *ASME Journal of Heat Transfer* 1991; **113**:48–56.
12. Ghia KN, Ghia U, Shih CT. Study of fully developed incompressible flow in curved ducts using a multigrid technique. *ASME Journal of Fluids Engineering* 1987; **109**:226–235.
13. Kamiyama Y, Mikami F, Ikui K, Hori T. Laminar forced convection heat transfer in curved channels of rectangular cross section. *Transactions of the JSME B* 1984; **50**:424–434.
14. Dong ZF, Ebadian MA. Numerical analysis of laminar flow in curved elliptic ducts. *ASME Journal of Fluids Engineering* 1991; **113**:555–562.
15. Thangum S, Hur N. Laminar secondary flows in curved rectangular ducts. *Journal of Fluid Mechanics* 1990; **217**:421–440.
16. Duh TY, Shih YD. Fully developed flow in curved channels of square cross-section inclined. *ASME Journal of Fluids Engineering* 1989; **111**:172–177.
17. Berger SA, Talbot L, Yao LS. Flow in curved pipes. *Annual Review of Fluid Mechanics* 1983; **15**:461–512.
18. Hatzikonstantinou P. A computational procedure for the incompressible three-dimensional parabolic flows. *Proceedings of the 4th GRACM Congress on Computer Mechanics*, Tsahalis (ed.), June 2002 University of Patras, Patras, Greece; 68–79.
19. Sakalis V, Hatzikonstantinou P. Predictions and accuracy of the CVP numerical method for the developed laminar flow in curved ducts. *Proceedings of the 4th GRACM Congress on Computer Mechanics*, Tsahalis (ed.), June 2002, University of Patras, Patras, Greece, vol. IV: 1400–1410.
20. Hirt CW, Cook JL. Calculating three-dimensional flow around structures and over rough terrain. *Journal of Computational Physics* 1972; **10**:324.
21. Chen WH, Jan R. The torsion effect on fully developed flow in helical square ducts. *Journal of Fluids Mechanics* 1993; **115**:292–301.
22. Bolinder CJ, Sunden B. Numerical prediction of laminar flow and forced convective heat transfer in a helical square duct with a finite pitch. *International Journal of Heat Mass Transfer* 1996; **39**:3101–3115.
23. Ghia KN, Ghia U, Shih CT. Study of fully developed incompressible flow in curved ducts using a multigrid technique. *ASME Journal of Fluids Engineering* 1987; **109**:226–235.
24. Joseph B, Smith EP, Adler RJ. Numerical treatment of laminar flow in helically coiled tubes of square cross section. *AIChE Journal* 1975; **21**(5):965–974.

